

Electrical equivalent model of symmetrical split ring resonator sensor-based microwave technology

Abstract. In this paper, a microwave planar sensor based on symmetrical split ring resonator (SSRR) is investigated. This sensor uses ring resonator with slits at 0° and 180° angles as method to realize the harmonic resonant frequency response and then, it integrated with symmetrical split ring for suppressing the undesired harmonic spurious. Compact size, simplicity, cost effective, and ease of fabrication are the main advantage of SSRR sensor. The model of analytical equivalent circuit is proposed and the characteristic of band-pass and band-stop are derived and investigated for the analysed SSRR with/without spurliners filters. The performance and sensitivity of the SSRR sensor is high with an average accuracy between 96% to 98 % at narrow band frequencies. This type of resonators sensors can detect the material properties under their chemical or physical changes which is essential for numerous applications such as quality control, agriculture, bio-sensing, medicine and pharmacy, food industry, and material science.

Streszczenie. Przedstawiono mikrofalowy czujnik planarny bazujący na symetrycznych pierścieniowych rezonatorach. Wykorzystano pierścieniowy rezonator ze szczeliną przy kącie 0° i 180° w celu uzyskania odpowiedniej częstotliwości rezonansowej. Zaproponowano schemat zastępczy czujnika skąd obliczono pasmo częstotliwości. Czujnik może być wykorzystywany do badania materiałów. **Model mikrofalowego czujnika wykorzystującego pierścieniowe rezonatory**

Keywords: Symmetrical split ring resonator (SSRR), Spurlines Filters, Equivalent circuit, Material characterization.

Słowa kluczowe: czujnik mikrofalowy, rezonator pierścieniowy

Introduction

Recently, the accuracy of material properties measurement can play a vital role in addressing the increased demand of industrial applications such as quality control in material science, in the food industry, and bio-sensing [1–8]. In the food industry, the originality of food composition is widely considered as main factor in the development of food industry. Uncertain ingredients in some frozen or junk food can cause allergy reaction. For example, the consumer may not know how to detect the mixture of pork meat and beef meat and whether the food is still fresh or not. There are some difficulties in permittivity characterization due to the coupling loss and low sensitivity of the sensor. Thus, there is a need in understanding of dielectric constant of materials, which is very important to numerous industries because it helps them to improve incoming inspection, helps them in manufacturing process monitoring, and also helps them to shorten design cycles.

For quality control, it is used purposely for checking the quality and safety of the food and agriculture which is been involved in seed treatment and grain drying in order to develop seed germination and insect control in stored grain by using high frequency and microwave electric field. It is also used for dairy products which is useful for roughly determining the content of the milk in terms of ionic compounds, fats, carbohydrates and proteins. On the other hands, it is used for fruits and vegetables because there is a need for rapid non-destructive quality measurements to know the freshness of fruits and vegetables. It is also used for Geo-science because when studying the dielectric properties of the soil it will be helpful for planting. Furthermore, it is used for bio-sensing in order to know the properties of tissue and cells and increase the knowledge for the processes of the biological at molecular level and it is also involved in current developments in radio frequency field and microwave hyperthermia for cancer treatment. Finally, it is used for pharmaceutical industries in order to check and validate the quality and safety of the medicine.

Dielectric properties relate to electric field and electric flux density where the polarization of a material is influenced by an electromagnetic field. The atoms and molecules of a material will be distorted and creating

effective dipoles with an electric dipole moment of P per unit volume when an electric field is applied [9, 10]. Both the electric flux density and electric field are related, and they can be expressed by:

$$(1) \quad D = \epsilon_0 E + P$$

where ϵ_0 is the free space permittivity of material. When the applied materials are linear and isotropic, the dipole moment P is in the same direction as E ($P=E$):

$$(2) \quad D = \epsilon_0 E + P \Rightarrow \epsilon_0 (1 + \chi_e) E = \epsilon_0 \epsilon_r E = \epsilon E$$

where ϵ is the permittivity of material and X_e is the electric susceptibility.

The electric behaviour of a materials with low conductivity is characterized by complex parameter known as permittivity (ϵ):

$$(3) \quad \epsilon = \epsilon' - j\epsilon''$$

Permittivity is dependent on the interaction of a measured material with the electric field which is applied on it. The interaction between the electric field and material is based on storage of energy and dissipation of energy. The lossless portion during exchange of energy between the field and energy is known as energy storage while absorbing electromagnetic energy by the material is known as energy dissipation. The real parts of the material (ϵ') describe storage while the imaginary parts of the material (ϵ'') describe the dissipation.

The units for permittivity is in Farads per meter (F/m), however, in microwave electronics are often dimensionless quantities relative permittivity (ϵ_r).

$$(3) \quad \epsilon_r = \frac{\epsilon}{\epsilon_0} \Rightarrow \frac{\epsilon' - j\epsilon''}{\epsilon_0} = \epsilon_r' - j\epsilon_r''$$

where ϵ_0 is the permittivity of the free space (8.854×10^{-12} F/m), ϵ_r' is the relative dielectric permittivity and ϵ_r'' is the loss factor [11]

Electrical characteristics which are dependent on dielectric properties are inherent in every material; accurate measurement of these properties helps engineers and

scientists to put the material to proper use for more solid designs and improved quality control. In electronics application, dielectric measurement is capable of providing critical design parameter information.

Therefore, further data collection is required to determine exactly the precise permittivity of materials which would be interesting to be used for material science and microwave engineering. Detecting the material properties under their chemical or physical changes is essential for numerous applications such as quality control, agriculture, bio-sensing, medicine and pharmacy, food industry, and material science [12–16].

In this paper, the first endeavour is to design a novel microwave planar sensor based on symmetrical split ring resonator (SSRR). This sensor uses ring resonator with slits at 0° and 180° angles as method to realize the harmonic resonant frequency response and then, it integrated with symmetrical split ring for suppressing the undesired harmonic spurious. Compact size, simplicity, cost effective, and ease of fabrication are the main advantage of SSRR sensor. The SSRR sensor provides a good performance at 2.2 GHz operating resonant frequency which is suitable for characterizing material properties at narrow band frequencies. This sensor achieved 97.17 % of the average accuracy for the measured standard MUT.

The second design involves the realization of harmonic suppression based on novel SSRR structure with spurline filters. The spurlines is devoted to the feed lines of SSRR structure in order to suppress undesired harmonic resonant frequency, hence resulting a small circuit size. The spurline filter offers numerous advantages such as compact size, suppressing undesired harmonic resonant frequency, and good electromagnetic shielding. The novel SSRR sensor with double spurline produced a narrowband with high sensitivity and achieved 98.38 % of the average accuracy of the measured standard MUT which can be used for various applications. While SSRR with single spurline produced high sensitivity with 96.55% achievement for the average accuracy of the measured standard MUT. It is almost certain that the proposed sensors will attribute to material characterization based complex permittivity for quality control and food industry applications.

Design Structure of Symmetrical Split Ring Resonator (SSRR)

The microwave planar resonators can be designed in any selective operating frequency for material characterizations as reported in [17–22] where they are operating at different frequencies of 1 GHz, 2.5 GHz, 1.28 GHz, 2.65 GHz, 10.66 GHz, 10.95 GHz and 2.44 GHz, respectively. This work is designed at selected operating frequency of 2.2 GHz for implementation and proof of concept where it can be customized for many important applications.

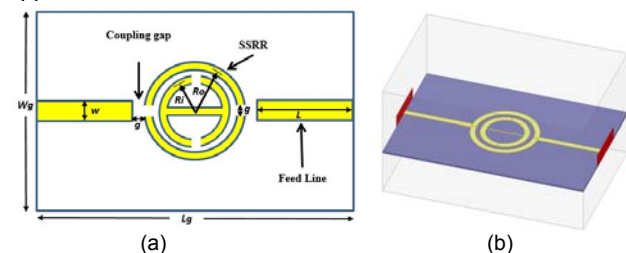


Fig.1. The symmetrical split ring resonator (SSRR) sensor: (a) structure design, (b) 3D model designed in HFSS. An example of the figure inserted into the text

The SSRR resonator device consists generally of printed microstrip on a rigid substrate. A two-layer board with one dielectric material is used, as demonstrated in

Fig.1. Roger corporation® RT/Duroid 5880 was used with substrate thickness of 0.787 mm (h), loss tangent of 0.0009 ($\tan\delta$), and permittivity of 2.20 (ϵ_r). It has a copper thickness of 17.5 μm (t). The designed parameters specifications for this SSRR sensor are specified in Table 1.

Table 1. The specification parameters of the SSRR sensor.

Parameter	Value	Parameter	Value
Substrate: Roger 5880	$\epsilon = 2.2, h = 0.787 \text{ mm}$ $t = 0.0175 \text{ mm}$	r	15.85 mm
f	2.2 GHz	w	2.5 mm
Zo	50 Ω	l	mm
Lg	103.14 mm	g	mm
Wg	68.3 mm		

Equivalent circuit of SSRR

The prototype of low-pass normally has system impedance of 1 Ω which means both the load impedance (Z_o) and generator impedance (Z_{in}) have a 50 Ω impedance. It is required to convert the impedance from 1 (ohm) impedance level to a load impedance level (Z_o). The scale for the impedances of all the circuit elements in the ring by 50 Ω as indicated in Fig.2.

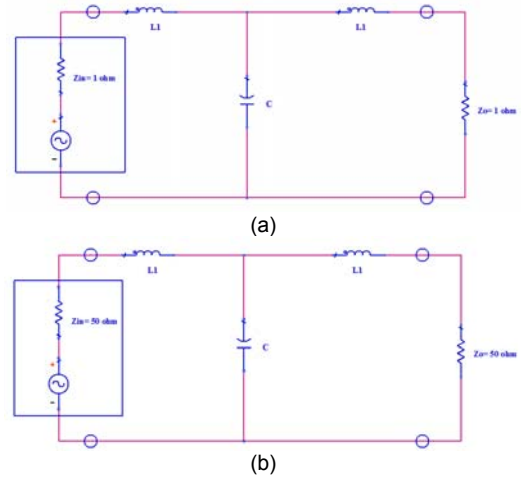


Fig.2. The impedance circuit for (a) low-pass prototype at impedance 1 Ω (b) low-pass prototype at impedance 50 Ω .

Thus, the inductances are multiplied by Z_o and capacitances are divided by Z_o [23]:

$$(4) \quad L \rightarrow Z_o L, \text{ and } C \rightarrow \frac{C}{Z_o}$$

Then, it is required to transform the low-pass prototype to bandpass prototype transformation with a center frequency and bandwidth. Fig.3 demonstrates the band-edges at $\omega = \pm 1$ in the low-pass prototype which converted to bandpass edges of bandwidth of ω_1 and ω_2 . The mid-band of the low-pass prototype at $\omega = 0$ must be converted to a center frequency in the bandpass filters.

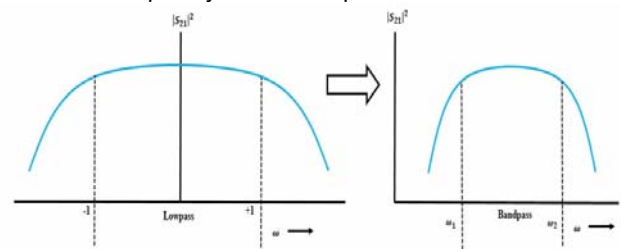


Fig.3. Low-pass prototype to bandpass prototype transformation.

This can be indicated as the following transformations [23]:

$$(5) \quad \omega \rightarrow \alpha \left(\frac{\omega}{\omega_0} - \frac{\omega_0}{\omega} \right)$$

For $w = -1$ and $w = +1$ to map to w_1 and w_2 then:

$$(6) \quad -1 = \alpha \left(\frac{\omega_1}{\omega_0} - \frac{\omega_0}{\omega_1} \right), \text{ and } +1 = \alpha \left(\frac{\omega_2}{\omega_0} - \frac{\omega_0}{\omega_2} \right)$$

Solving the equations before, simultaneously

$$(7) \quad \omega_0 = \sqrt{\omega_1 \omega_2}, \text{ and } \alpha = \frac{\omega_0}{\omega_2 - \omega_1}$$

where the $\omega_0 = 2\pi f_0$ is the mid-band frequency and the α is the scaling factor of bandwidth.

By applying the transformation to a series inductor as indicated in Fig.4 for the connected series impedance of LC circuit [23]:

$$(8) \quad Z = j\omega L = j\alpha L \left(\frac{\omega}{\omega_0} - \frac{\omega_0}{\omega} \right) = j \left(\frac{\alpha L}{\omega_0} \right) \omega - \frac{j}{\omega \left(\frac{\alpha L \omega_0}{1} \right)}$$



Fig.4. Inductance transformation from low-pass to bandpass prototype.

However, for applying the transformation to a capacitor of admittance $j\omega C$ as shown in Fig.5, for the parallel connected admittance of LC circuit [23]:

$$(9) \quad Y = j\omega C = j\alpha C \left(\frac{\omega}{\omega_0} - \frac{\omega_0}{\omega} \right) = j \left(\frac{\alpha C}{\omega_0} \right) \omega - \frac{j}{\omega \left(\frac{1}{\alpha C \omega_0} \right)}$$

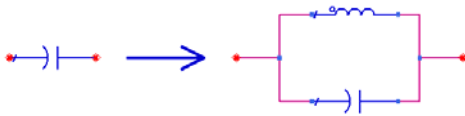
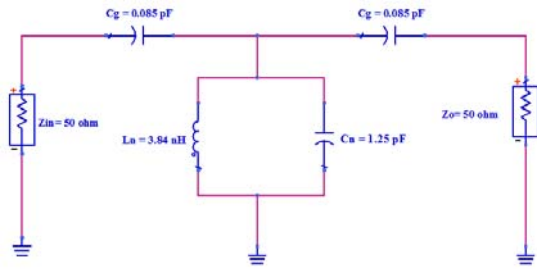
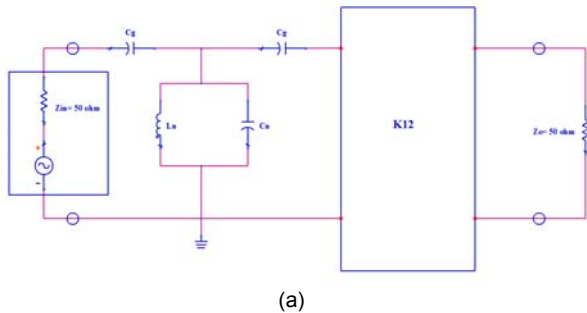


Fig.5. Capacitance transformation from low-pass to bandpass prototype.

The bandpass filter prototype equivalent circuit is used to produce a single-mode filter in ring resonator as shown in Fig.6. The C_g represent the coupling gap mechanism between the feedlines and the ring resonator. Similarly, the 2nd and 3rd and 4th harmonic modes of the ring resonator equivalent circuit can be analogically developed of the bandpass prototype circuit as indicated in Fig.7. The analogical equivalent circuit of the harmonic modes can be also developed based on a parallel combination of two, three and four single-mode equivalent circuits respectively.



(b)

Fig.6. Single-mode circuit of ring resonator (a) Bandpass prototype using K inverter (b) Bandpass prototype of fundamental frequency (1st resonance frequency).

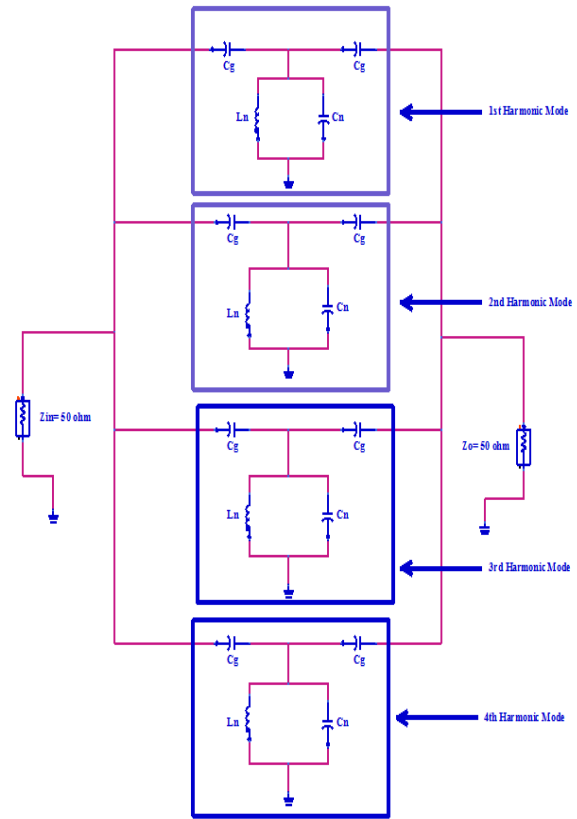


Fig.7. Equivalent circuit of analogically first four modes for the SSRR resonator at different harmonics frequencies.

The characteristic admittance of inverter and the capacitance (C_r) value of the bandpass prototype can be determined using [23]:

$$(10) \quad C_r = \frac{2}{\eta} \sin \left[\frac{(2r-1)\pi}{2N} \right]$$

where: $\eta = \sinh \left[\frac{1}{N} \sinh^{-1} \left(\frac{1}{\epsilon} \right) \right]$, ϵ is the insertion loss ripple.

The ring equivalent circuit can be transformed from the bandpass prototype equivalent circuit using [23]:

$$(11) \quad L_n = \frac{1}{C_r \omega_0}, \text{ and } C_n = \frac{C_r}{\omega_0} - \frac{\sqrt{\alpha-1}}{\alpha \omega_0} - C_{r,r+1}$$

where L_n is the inductance value of n th shunt inductor, and C_n is the inductance value of n th shunt capacitor, and N is the number of harmonic modes,

$$C_{r,r+1} = \frac{K_{r,r+1}}{\omega_0}, \quad \alpha = \frac{\omega_0}{\omega_2 - \omega_1}, \quad \text{and } K_{r,r+1} = \sqrt{\frac{\eta^2 + \sin^2 \left(\frac{r\pi}{N} \right)}{\eta}}$$

The simulated frequency response of the equivalent circuit of single mode and the four harmonic modes are shown in Fig.8.

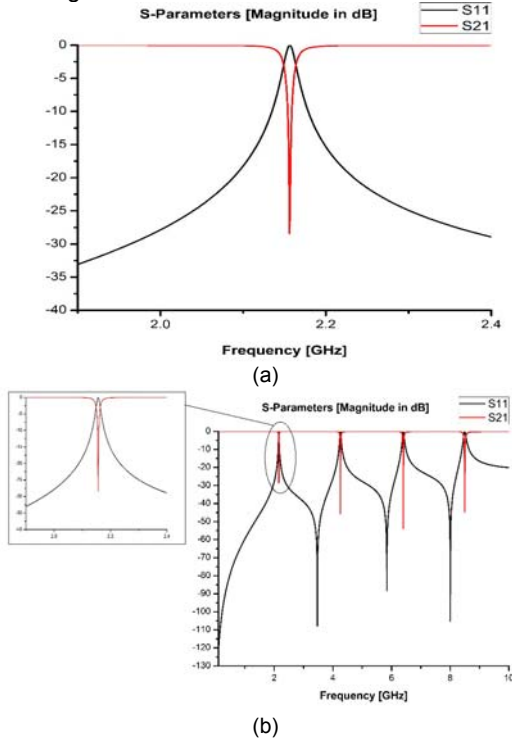


Fig.8. Simulated response of a capacitively coupled bandpass filter (a) single mode (b) First four harmonic modes.

Design Structure of SSRR with Spurlines

Generally, the bandstop filter is applied to reject undesired signal at selective frequency and block the spurious signal in RF and microwave systems [24, 25]. Fig.9 depicts the conventional schematic view of spurlines, which work as a band-stop filter. The design configuration is embedded and etched by L-shape slot which has (a) as length and (s) as capacitive gap width. The undesired wavelength can be found [26]:

$$(12) \quad a = \frac{\lambda_g}{4}$$

where a is the length of spurline, and λ_g is the undesired wavelength.

After derivation of equation (12) and convert it into the frequency domain, it can be as [26]:

$$(13) \quad f_{stop} = \frac{c}{4a\sqrt{\epsilon_{eff}}}$$

where a is the length of spurline, c is the light speed (3×10^8 m/s), ϵ_{eff} is the substrate effective permittivity, and f_{stop} is the undesired or rejected frequency.

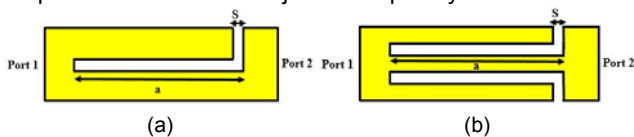


Fig.9. The schematic diagram for spurlines filters (a) single spurline (b) Double spurline.

While Fig.10 illustrates the schematic view of 3D model for SSRR with both single and double spurlines filter by using High Frequency Structure Simulator (HFSS). The designed parameters specifications for the SSRR design with spurlines are demonstrated in Table 2.

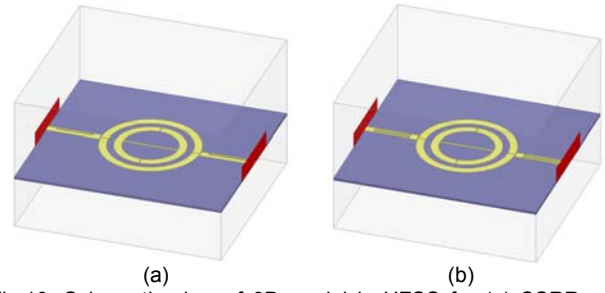


Fig.10. Schematic view of 3D model in HFSS for (a) SSRR with single spurline (b) SSRR with double spurline.

Table 2. Design parameters specification for SSRR with spurlines filters.

Parameter	Value	Parameter	Value
Substrate: Roger5880	$\epsilon = 2.2$	r	15.85 mm
f	2.2 GHz	t	0.0175 mm
Zo	50 Ω	w	2.5 mm
Lg	71.84 mm	l	34.0 mm
Wg	68.3 mm	g	0.37 mm
h	0.787 mm	a	12.76 mm

Equivalent Circuit of SSRR with Spurlines

Both types of spurlines can be modeled as one parallel LCR resonator. One LC resonator modeled the resonant frequencies and the effect of radiation and loss of transmission are considered as a resistor (R). According to the theory of transmission line and the approach of spectral domain [23], the circuit elements can be extracted using a transformation of low-pass prototype to band-stop prototype. Thus, for the equivalent circuit, it is required to convert the low-pass prototype to band-stop prototype transformation with a center frequency and bandwidth. Fig.11 demonstrates the band-edges at $\omega = \pm 1$ in the low-pass prototype which converted to band-stop edges of bandwidth of ω_1 and ω_2 . In this case, the zero transmission at infinity in a prototype of low-pass that have to be mapped to the center of the stopband of filter.

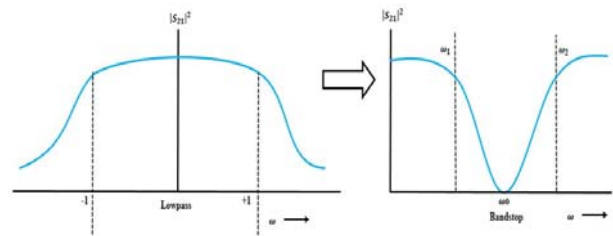


Fig.11. Low-pass prototype to band-stop prototype transformation.

This can be indicated as the following transformations [23]:

$$(14) \quad \omega \rightarrow \frac{-1}{\alpha \left(\frac{\omega}{\omega_0} - \frac{\omega_0}{\omega} \right)}$$

$$\text{where: } \omega_0 = \sqrt{\omega_1 \omega_2}, \quad \alpha = \frac{\omega_0}{\omega_2 - \omega_1}$$

The capacitor is converted into a series combination of inductor L' and capacitor C' where:

$$(15) \quad L' = \frac{\alpha}{\omega_0 C}, \quad \text{and} \quad C' = \frac{C}{\alpha \omega_0}$$

In case of bandpass filters, the realizable element values of narrow bandwidths by scaling network so that the couplings become relatively weak. However, in case of

narrowband band-stop filter design, the impedance of inverter must remain at unity impedance so that the filter has a broad passband. Fig.12 demonstrates LC circuit connection of band-stop for capacitively coupled resonator to control the impedance level.

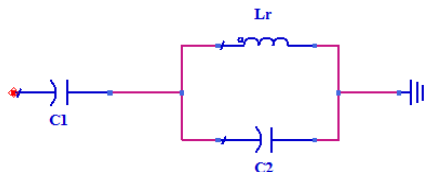


Fig.12: LC connection of band-stop prototype.

The inductor (L_r) value can be assumed for physical realizability and C_1 and C_2 are found for the band-stop prototype equivalent circuit using [23]:

$$(16) \quad C_1 = \sqrt{\frac{C_r}{\omega_0^2 L_r \alpha}}, \text{ and } C_2 = \frac{1}{\omega_0^2 L_r} - C_1$$

where: C_1 and C_2 are the capacitor values in the n th resonator

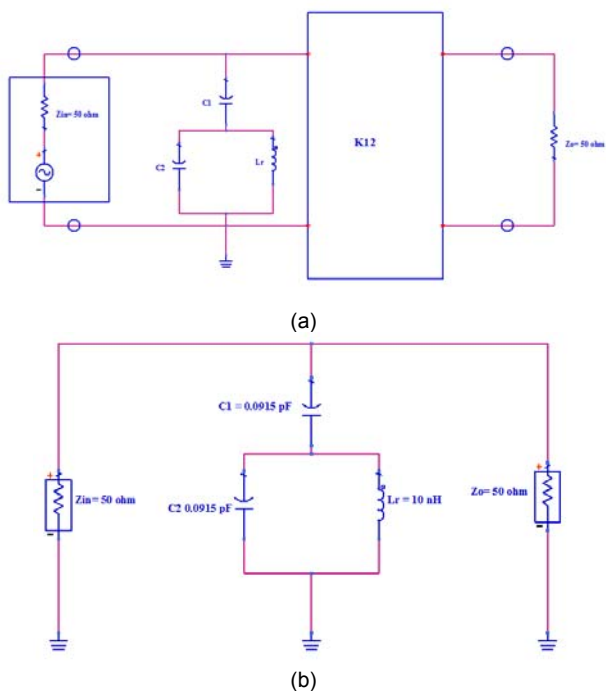


Fig.13. Single-mode circuit of band-stop spurlines filters (a) Band-stop prototype using K inverter (b) Band-stop prototype of fundamental frequency.

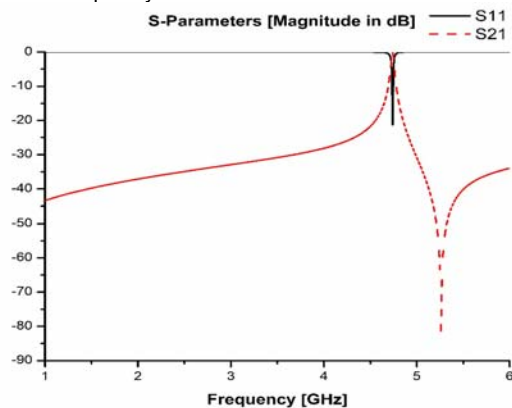


Fig.14. Simulated response of a capacitively coupled band-stop filter.

By considering all inductors to have a physically realizable value of 10 nH in band-stop prototype of $50 \text{ }(\Omega)$ system, the low-pass prototype system will have an inductor value of 0.2 nH . The band-stop filter prototype equivalent circuit is used to produce a single-mode filter in ring resonator as shown in Fig.13. The simulated frequency response of the equivalent circuit is shown in Fig.14.

Fabrication and Measurement Process

After the results show a good response and satisfied, the fabrication hardware will be done which involves generating mask transparent, filming, photo exposure process, etching process, and soldering the SMA connectors. The design structures are transferred from EM simulation tools known as High Frequency Structure Simulator (HFSS) to Corel draw software then printed onto photo paper. Then, etching process will be implemented for removing the unwanted conductor copper in etching container using chemical substance. Once the fabrication is done, the ports will be soldered along with the SMA connectors. Then, all measurement will be performed using Vector Network Analyzer (VNA) to measure the S-parameters (S_{21}) for the designed device under test (DUT). Fig.15 demonstrates the connection of the device under test (DUT) to VNA for measurement process.

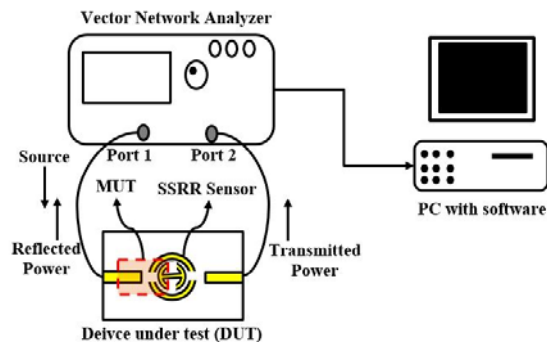


Fig.15. Connection of DUT and VNA for measurement process.

Finally, the material under test (MUT) used as standard materials under test are listed in Table 3. They will be tested in the designed devices for verifications and validations. Four standard materials namely air, Roger 5880, Roger 4350, and FR4 will be used to model and fit the dependence of resonant frequency on dielectric permittivity using 2nd order polynomial. Then, the unknown material under test (MUT) will be determined. Fig.16 depicts the fabricated SSRR sensor with unknown permittivity of the overlay material under test (MUT) for measuring and characterizing the properties of the materials.

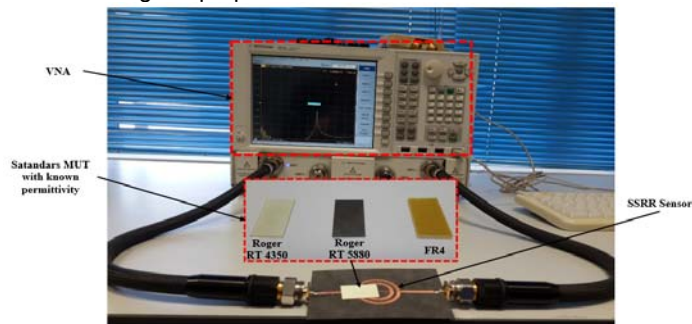


Fig.16. Fabricated SSRR sensor with the measurement of the unknown material under test (MUT).

Table 3. Standards material under test (MUT) with known permittivity

Literature [ϵ_r]	Material under test (MUT)			
	Air	Roger 5880	Roger 4350	FR4
	1	2.2	3.48	4.4

Results and discussion

For the conducted experiment, the resonance frequency is shifted to lower frequency. This shift is directly proportional to the permittivity of the dielectric MUT. The relationship between the frequency (f_o) and the permittivity (ϵ_r) can be modeled by curve fitting method which is 2nd order polynomial as indicated in expression (18):

$$(17) \quad \epsilon_r = af_o^2 + bf_o + c$$

Where the coefficients a, b, c can be found by using standard materials under test (MUT) such as Air, Roger RT 5880, Roger 4350, and FR4 of which the dielectric properties are well known.

The behavior response of the loaded SSRR sensor with standard MUT is demonstrated in Fig.17. It can clearly be seen that the resonant frequency is changed for each MUT with known dielectric constant. For each tested material, the resonant frequency is slightly shifted to lower frequency which depends on the permittivity of MUT as indicated in Fig.17. This makes the SSRR sensor detect and characterize numerous materials with a very small variation range of materials permittivity.

Table 4. Summary of experimental results for the SSRR sensors and commercialized coaxial probe kit sensor.

MUT	Refer- ence, ϵ_r	Accuracy of measured permittivity by using							
		Commercializ-ed Coaxial Probe Kit sensor		This work					
		ϵ_r	% ϵ_r	Normal SSRR		SSRR with single spurline		SSRR with double spurlines	
Air	1	1.11	89.00	ϵ_r	% ϵ_r	ϵ_r	% ϵ_r	ϵ_r	% ϵ_r
Roger 5880	2.2	2.34	93.64	0.94	94.00	0.95	95.00	0.96	96.00
Roger 4350	3.48	3.4	97.70	2.12	96.37	2.32	94.55	2.23	98.63
FR4	4.4	4.22	95.91	3.50	99.43	3.38	97.13	3.45	99.13
				4.45	98.86	4.42	99.55	4.41	99.77

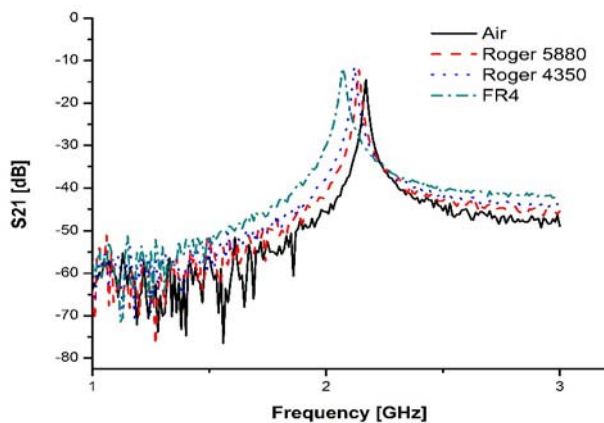


Fig.17. Changes in resonance frequency when known permittivity of MUT is tested.

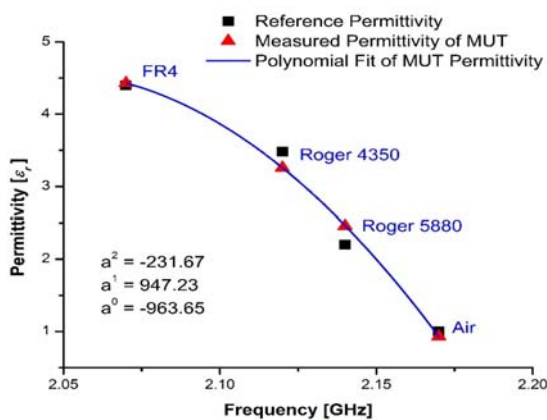


Fig.18. The mathematical modelled for the measured permittivity of MUT in comparison with the reference permittivity using SSRR sensor.

Four MUT such as Air, Roger Duriod RT 5880, Roger 4350 and FR4 were used as calibration samples since their dielectric constant is well known, in order to observe the changes in resonant frequency and the relation to the permittivity of materials. Thus, the materials with unknown permittivity can be extracted. After the modelling the change of resonant frequency on permittivity mathematically using Origin v.8 software based on regression analysis 2nd order polynomial technique, the unknown permittivity of materials can be determined and extracted accordingly. Fig.18 demonstrates the numerical model for the resonant frequency measurement with respect to the tested permittivity of MUT. It is apparent the resonant frequency is in a great fit to the reciprocal of the permittivity of the materials. The mathematical modelled for the measured permittivity of MUT is expressed as follows:

$$(18) \quad \epsilon_r = -231.67 f^2 + 947.23 f - 963.65$$

Validation with Commercialized Coaxial Probe Kit Sensor in Laboratory

In this section, we compare the measurement results of the proposed sensors with the commercialized coaxial probe-kit sensor which is available in laboratory. The comparison is based on the accuracy and sensitivity during testing standard materials with known permittivity. Fig.19 illustrates the measured permittivity of material under test for Air (permittivity = 1), Roger RT 5880 (permittivity = 2.2), Roger 4350 (permittivity = 3.48), and FR4 (permittivity = 4.4) by using Coaxial Probe-Kit sensor. A comparison of the measured permittivity between the proposed sensors and commercialized coaxial probe kit sensor is tabulated in Table 4 at normal room temperature condition. The comparison is based on the standard permittivity of the tested materials properties for both the designed SSRR sensor and the commercialized sensor. It is apparent from this table that the proposed sensors have a better accuracy and sensitivity. Fig.20 indicates the accuracy and sensitivity of the proposed sensor and the commercialized coaxial

probe kit sensor when compared them to the reference permittivity.

The SSRR sensor with and without spurlines filters are developed to detect and characterize solid or/mixture materials based on low cost with high sensitivity and accuracy. The presented sensors in this thesis are compared to the commercialized coaxial probe kit sensor and those found in literatures. It can be observed that our sensors have much more sensitivity and accuracy compare to others. Not only this but also in terms of the cost, they are inexpensive to build due to the ease of fabrication and compactness in circuit size.

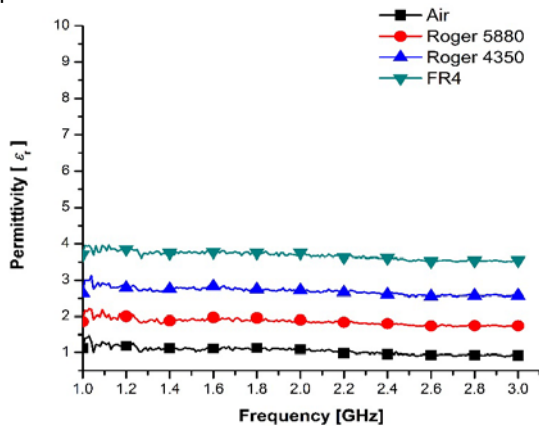


Fig.19. The measured permittivity of the standard materials by using commercialized Coaxial Probe-Kit sensor.

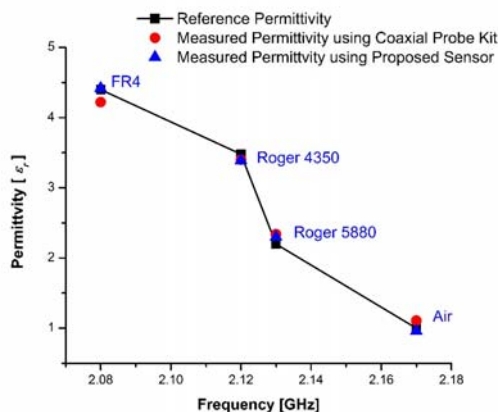


Fig.20. Comparison of the SSRR sensor and commercialized Coaxial Probe Kit sensor measurement in terms of accuracy and sensitivity.

Conclusion

The procedures of designing a novel symmetrical split ring resonator (SSRR) with/without spurlines have been explained in detail in this chapter. The designed SSRR sensor is based on microstrip planar resonator. The effects of coupling gap have been investigated and proposed enhancement techniques. The electric field distributions and the location of the material under test (MUT) have been also demonstrated. The fabrication and measurement setup have also been discussed thoroughly. Using a specific experimental methodology, tests of four standard materials with known permittivity and two materials with unknown material will be performed to demonstrate the SSRR sensor ability of characterizing the properties of materials. Accordingly, the numerically established relations will be experimentally verified for these references materials and the results of simulation and measurement will be discussed in next chapter.

Acknowledgment

This work was sponsored and supported by UTeM Zamalah Scheme and Universiti Teknikal Malaysia Melaka (UTeM).

Authors: Rammah A. Alahnomi¹, Zahriladha Zakaria², Zulkalnain Mohd Yusoff³, Ammar Alhegazi⁴, Hussein Alsariera⁵, Norhanani Abd Rahman⁶

Microwave Research Group, Centre for Telecommunication Research and Innovation (CeTRI), Faculty of Electronics and Computer Engineering, Universiti Teknikal Malaysia Melaka (UTeM), 76100 Durian Tunggal, Melaka, Malaysia.

Corresponding author: Prof. Dr. Zahriladha Zakaria, E-mail:

zahriladha@utem.edu.my².

Authors E-mail:

alammah89@gmail.com¹,

zulkalnain@utem.edu.my³,

ammarhejazy@hotmail.com⁴,

husseinsareira@gmail.com⁵,

norhanani80@gmail.com⁶

REFERENCES

- [1] Kang, B.,; Cho, J.,; Cheon, C., and Kwon, Y.,: Nondestructive Measurement of Complex Permittivity and Permeability Using Multilayered Coplanar Waveguide Structures, IEEE Microw. Wirel. Components Lett., **15** (2005), no. 5, pp. 381–383.
- [2] Ansari, M.A.H.,; Jha, A.K., and Akhtar, M.J.,: Permittivity Measurement of Common Solvents Using the CSRR Based Sensor, Antennas Propag. Usn. Natl. Radio Sci. Meet. 2015 IEEE Int. Symp., **1** (2015), no. 2, pp. 1199–1200.
- [3] Boybay, M.S., and Ramahi, O.M.,: Non-Destructive Thickness Measurement Using Quasi-Static Resonators, IEEE Microw. Wirel. Components Lett., **23** (2013), no. 4, pp. 217–219.
- [4] Alahnomi, R.A.,; Zakaria, Z.,; Ruslan, E.,; Rashid, S.R.A.,; Azuan, A., and Bahar, M.,: High - Q Sensor Based on Symmetrical Split Ring Resonator with Spurlines for Solids Material Detection, (2017), no. c.
- [5] Alahnomi, R.A.,; Zakaria, Z.,; Ruslan, E.,; Rashid, S.R.A.,; Azuan, A.,; Bahar, M., and Shaaban, A.,: Microwave Biosensor Based on Symmetrical Split Ring Resonator with Spurlines Filters for Therapeutic Goods Detections, PLoS One, (2016).
- [6] Azuan, A.,; Bahar, M.,; Zakaria, Z.,; Rosmaniza, S.,; Rashid, A., and Isa, A.A.,: Microstrip Planar Resonator Sensors for Accurate Dielectric Measurement of microfluidic solutions, 3rd Int. Conf. Electron. Des., (2016), pp. 416–421.
- [7] Alahnomi, R.,; Binti, N.,; Hamid, A.,; Zakaria, Z.,; Sutikno, T., and Azuan, A.,: Microwave Planar Sensor for Permittivity Determination of Dielectric Materials, **11** (2018), no. 1, pp. 362–371.
- [8] Alahnomi, R.A.,; Zakaria, Z.,; Ruslan, E., and Isa, A.A.M.,: Optimization Analysis of Microwave Ring Resonator for Bio-sensing Application, Int. J. Appl. Eng. Res., **10** (2015), no. 7, pp. 18395–18406.
- [9] Collin, R.E.,: Foundations for Microwave Engineering, 2nd Editio ed., IEEE Press Series On Electromagnetic Wave Theory, 2001.
- [10] Saeed, K.,: Microwave Materials Characterisation using Planar Resonant Sensors, Univ. Leeds, (2008), no. July.
- [11] Chen, L.F.,; Ong, C.K.,; Neo, C.P.,; Varadan, V. V, and Varadan, V.K.,: Microwave electronics: measurement and materials characterization, John Wiley & Sons Ltd, 2004.
- [12] Kulkarni, S., and Joshi, M.S.,: Design and Analysis of Shielded Vertically Stacked Ring Resonator as Complex Permittivity Sensor for Petroleum Oils, IEEE Trans. Microw. Theory Tech., **63** (2015), no. 8, pp. 2411–2417.
- [13] Von, A.R., and Hippe.,: Dielectric Materials and Applications, Massachusetts Institute of Technology. John Wiley and Sons, no date.
- [14] Shaji, M., and Akhtar, M.J.,: Microwave coplanar sensor system for detecting contamination in food products, IEEE MTT-S Int. Microw. RF Conf., (2013), pp. 1–4.
- [15] Jha, A.K., and Jaleel Akhtar, M.,: Automated RF measurement system for detecting adulteration in edible fluids, 2013 IEEE Appl. Electromagn. Conf., (2013), no. 1, pp. 1–2.
- [16] Celik, N.,; Gagarin, R.,; Huang, G.C.,; Iskander, M.F., and Berg, B.W.,: Microwave Stethoscope: Development and Benchmarking of a Vital Signs Sensor Using Computer-Controlled Phantoms and Human Studies, IEEE Trans. Biomed. Eng., **61** (2014), no. 8, pp. 2341–2349.

- [17] Jilani, M.T.; Wen, W.P.; Zakariya, M.A., and Cheong, L.Y.: Dielectric Method for Determination of Fat Content at 1 GHz Frequency, *IEEE*, (2014), pp. 2–5.
- [18] Abduljabar, A.; Yang, X.; Barrow, D., and Porch, A.: Microstrip Split Ring Resonator for Microsphere Detection and Characterization, *Microw. Symp. (IMS), 2015 IEEE MTT-S Int.*, (2015), pp. 1–4.
- [19] Boybay, M.S., and Ramahi, O.M.: Material Characterization Using Complementary Split-Ring Resonators, *IEEE Trans. Instrum. Meas.*, **61** (2012), no. 11, pp. 3039–3046.
- [20] Ansari, M.A.H.; Jha, A.K., and Akhtar, M.J.: Design and Application of the CSRR Based Planar Sensor for Non-Invasive Measurement of Complex Permittivity, *IEEE Sens. J.*, (2015), no. c.
- [21] Zhou, J.; Jia, P.; Zhang, Y., and He, X.: High sensitive biosensor based on aSRR and high-impedance microstrip line, *2nd Int. Conf. Meas. Inf. Control*, (2013), pp. 234–237.
- [22] Kulkarni, S., and Joshi, M.S.: Design and Analysis of Shielded Vertically Stacked Ring Resonator as Complex Permittivity Sensor for Petroleum Oils, *IEEE Trans. Microw. Theory Tech.*, **63** (2015), no. 8, pp. 2411–2417.
- [23] Hunter, I.: *Theory and Design of Microwave Filters*, First edition., The Institution of Engineering and Technology, 2001.
- [24] Zobilah, A.M.; Othman, A.; Shairi, N.A., and Zakaria, Z.: Parametric studies of ring and parallel coupled line resonators for matched bandstop filter design, **14** (2019), no. 1, pp. 29–37.
- [25] Zobilah, A.M.; Shairi, N.A.; Zakaria, Z.; Ahmad, B.H.; Zahari, M.K., and Wong, P.W.: Simulation Analysis on the Potential Application of Matched Bandstop to Bandpass Filter in Filter Integrated SPDT Switch Design, **10** (2018), no. 4, pp. 127–131.
- [26] Angkawisittpan, N.: Miniaturization of bandstop filter using double spurlines and double stubs, *Przeegląd Elektrotechniczny (Electrical Rev.)*, (2012), no. 11, pp. 178–181.